KNS Spring Meeting 2025

Theoretical and Experimental Investigation of Radium Adsorption Mechanisms on Engineered Barrier Material

공학적 방벽 완충재의 라듐 흡착 메커니즘에 대한 이론 및 실험 연구

Author: Jaeeun Kang* and Wooyong Um

Jaeeun Kang*

Nuclear Environmental Laboratory (NEL)
Division of Advanced Nuclear Engineering (DANE), POSTECH

2025년 5월 22일 제주 국제컨벤션 센터

CONTENTS

Nuclear Environmental Lab.

Engineered barrier system

Deep geological disposal

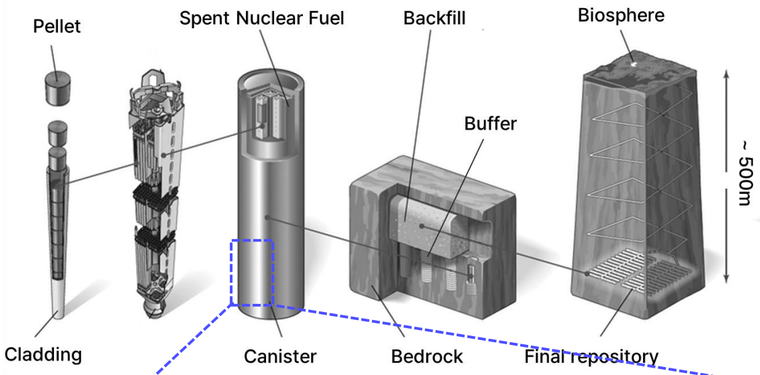

❖ Engineered Barrier System (EBS)

1. Pellet
2. Cladding tube
3. Canister with copper and iron
4. Buffer material with bentonite
5. Bedrock

Corrosion of spent nuclear fuel

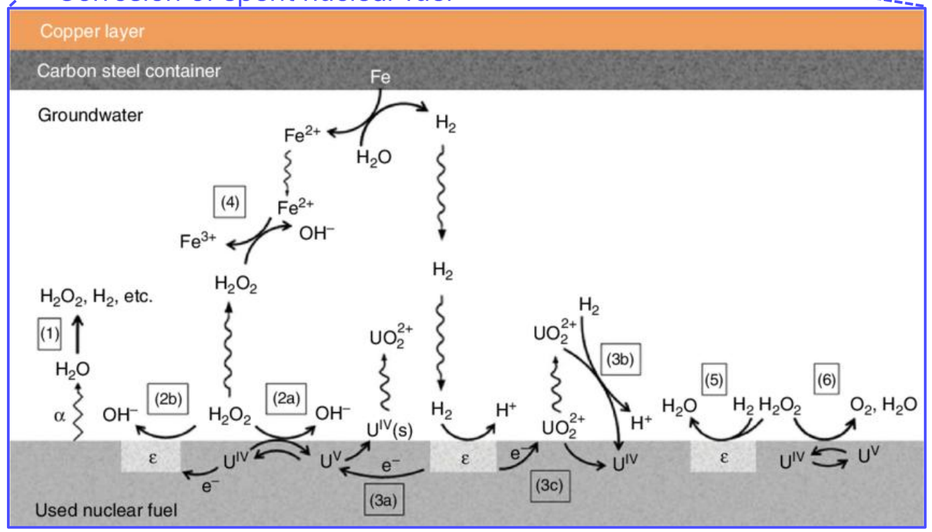

Figure 1*. Schematic illustration of the reactions included in the model for the α-radiolytic corrosion of spent nuclear fuel.

Thermo-Hydro-Mechanical-Chemical (THMC) processes

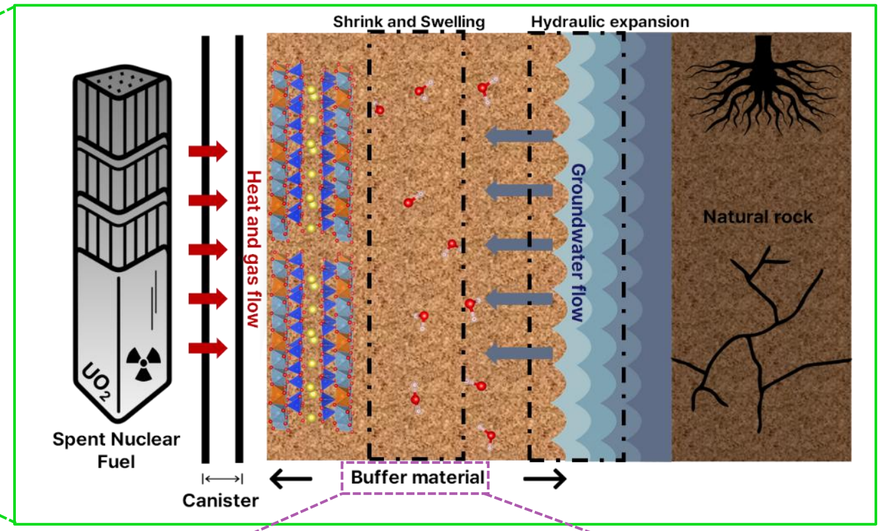

Buffer materials

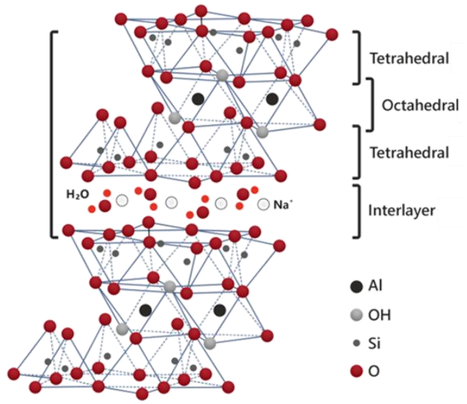

❖ Buffer materials properties

1. Hydraulic conductivity ↓
2. Retention capacity ↑
3. Cation exchange capacity ↑
4. Swelling potential ↑
5. Thermal conductivity ↑

Figure 2. Schematic illustration of sodium montmorillonite structure.

*Ref: Liu, N., et al., Predicting radionuclide release rates from spent nuclear fuel inside a failed waste disposal container using a finite element model. *Corrosion*, 75(3), 2019.

Behavior of radionuclides from spent nuclear fuel

Various cases of barrier functions*

❖ Scenarios based on potential loss of safety functions

Technical report for long-term safety

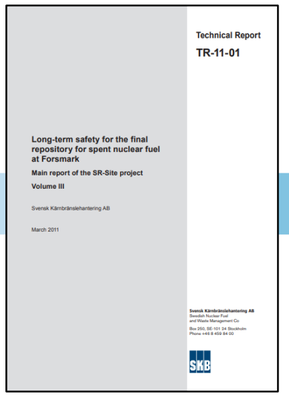
Technical Report
TR-11-01

Long-term safety for the final repository for spent nuclear fuel at Forsmark
Main report of the SR-Site project
Volume III

Svensk Kärnbränslehantering AB

March 2011

Various barrier function scenarios

Select 6 additional scenarios based on safety functions:
3 relating to failed states of the buffer
3 relating to failed states of the canister

Analyse occurrence of:

"Advective" buffer Buff1ab, Buff5 R1bc, R2ab	Frozen buffer Buff6b R4a	Transformed buffer Buff4 R1de, R2ab

Propagate each of these (descriptions of buffer states) to analysis of each of:

Canister failure due to corrosion Can1, Buff1 R1adf , R2ab + §	Canister failure due to isostatic load Can2 R3a + §	Canister failure due to shear load Can3, Buff3 R3bc + §

§ safety functions related to propagated buffer states included indirectly

Assumption of extreme case

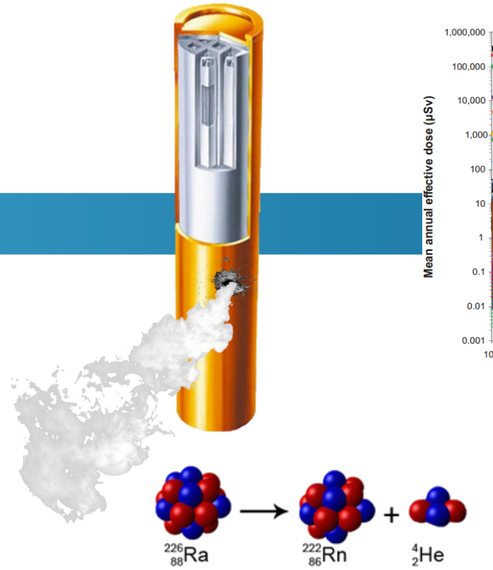

Near and Far-field mean annual effective dose

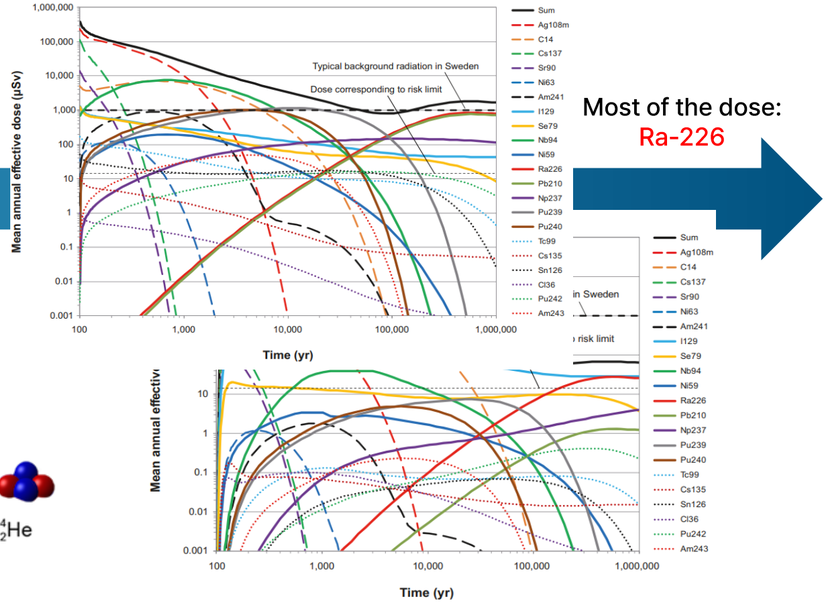

Most of the dose:
Ra-226

Figure 3. Mean annual effective dose in near and far fields from spent nuclear fuel under an extreme scenario for long-term safety assessment.

❖ Spent nuclear fuel composition

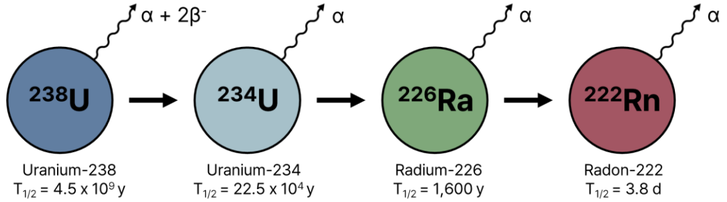

"By integrating computational and experimental approaches, this study aims to investigate the Ra adsorption on the buffer material of engineering barriers†."

†Kang, J., et al., *Applied Surface Science*, 703, 163406 (2025).

*Ref: Svensk Karnbranslehantering AB, Long-term safety for the final repository for spent nuclear fuel at Forsmark Main report of the SR-Site project, Volume III (Technical Report TR-11-01), 2011.

Materials and methods

Materials and methods

- Adsorbent: Bentonil-WRK
- Converted to Na-exchanged MMT through treatment with a 1 M $NaNO_3$.
- Contact time: 72 hours
- Solution to solid ratio: 0.01 g/mL for Ra and Ba.
- Analytics instruments: LSC and ICP-MS

Table 1. Mineralogical composition of raw Bentonil.

Sample No.	Montmorillonite	Albite	Quartz	Cristobalite
1	76.8	9.6	-	13.7
2	76.7	8.7	1.4	13.3
3	77.0	9.4	-	13.6

Characterization of Adsorbent Materials

X-Ray Diffraction (XRD) and BET

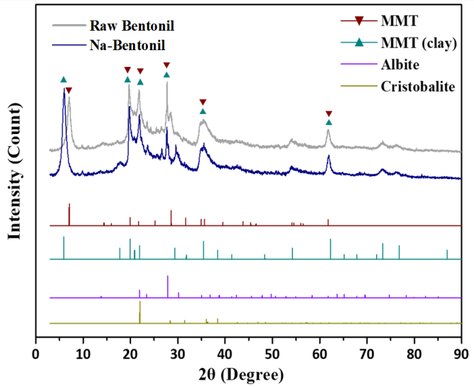

Figure 4. XRD patterns of raw and Na-Bentonil samples.

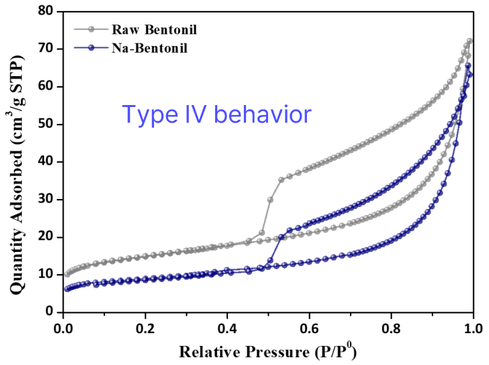

Figure 5. Isotherm linear plot of N_2 adsorption/desorption for raw and Na-MMT.

Scanning Electron Microscopy-Energy Dispersive Spectrum (SEM-EDS)

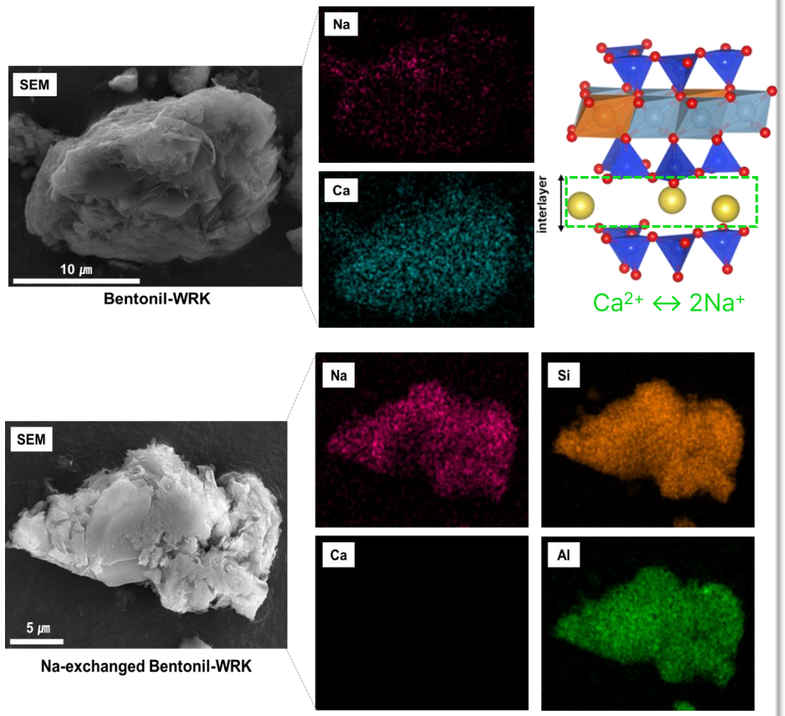

Figure 6. SEM-EDS analysis of raw and Na-Bentonil.

Batch adsorption experiment

Radioactive Isotope (Radium-226)

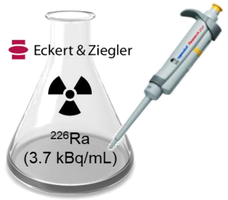

- **Batch adsorption experiment**

1. Isotherm studies were conducted at pH 6.7 using solutions with radioactivity ranging from 5-50 Bq/mL.
2. The effect of pH on Ra adsorption was evaluated using ^{226}Ra (15 Bq/mL) across a pH range of 2 to 11.

- **Detection efficiency (ε)**

Liquid scintillation counter

Due to the decay of ^{226}Ra into its daughter nuclides (^{222}Rn, ^{218}Po, and ^{214}Po), the detection efficiency can reach 300%.

$$\varepsilon = \frac{N_{net}}{A_{Ra226}(1 - e^{-\lambda t})}$$

where N_{net} is net count rate (cps) and A_{Ra226} is ^{226}Ra radioactivity (Bq), λ is decay rate of ^{222}Rn (d^{-1}), and t is time period from separation to measurement (d), respectively.

Equation 1. Detection efficiency(ε)

Batch adsorption experiments using Ba (from $BaNO_3$) as a surrogate for Ra were performed to extend the Ra adsorption study, including dosage, kinetics, isotherm, pH, and ionic strength effects.

Results and discussions

Ra adsorption results for isotherm, pH, and ionic strength

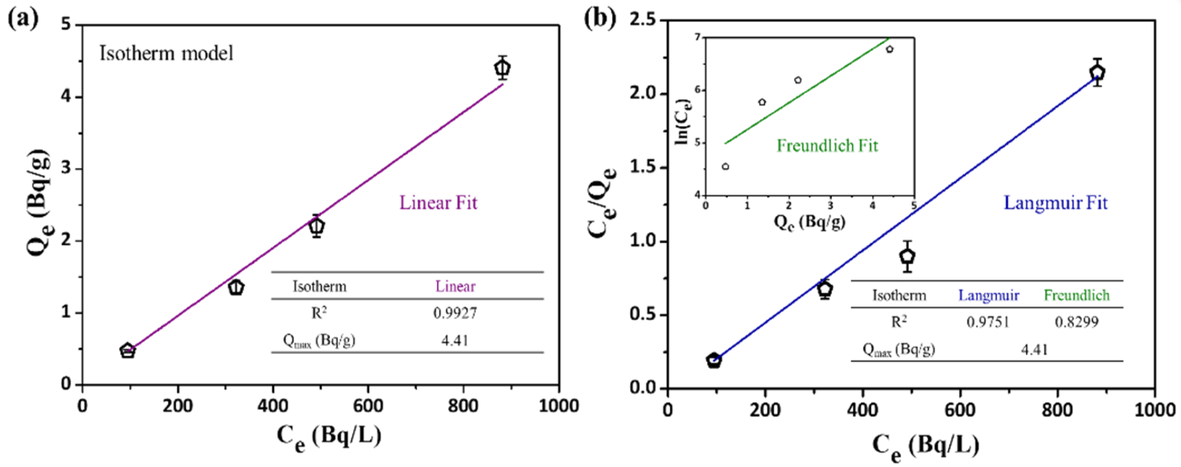

Figure 7. (a) Linear isotherm model and (b) Langmuir and Freundlich models of Ra adsorption on Na-Bentonil.

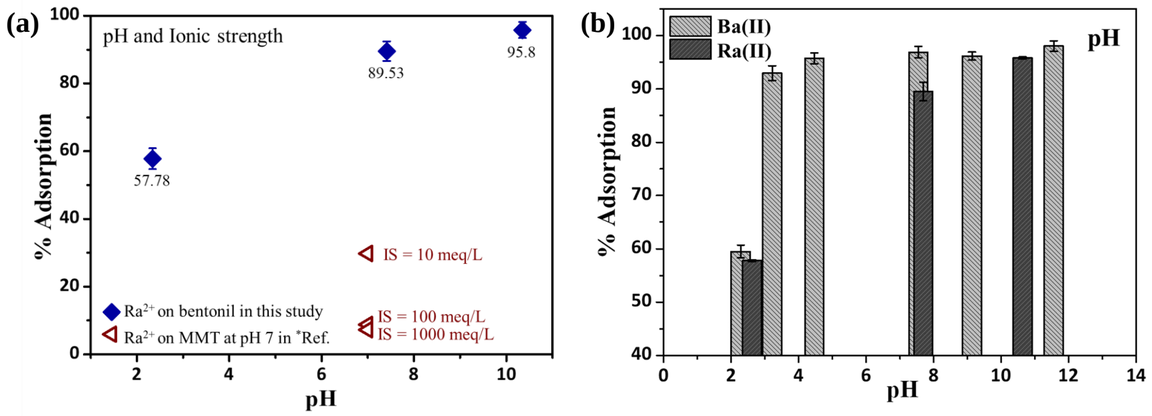

Figure 8. (a) Adsorption behavior of Ra^{2+} on MMT as a function of pH and ionic strength (Initial Ra radioactivity: 15 Bq/mL; *ionic strength effects discussed based on *Ref.); (b) Comparison of adsorption rates of Ba and Ra on Na-Bentonil at different pH;

Ba adsorption results for isotherm, pH, and ionic strength

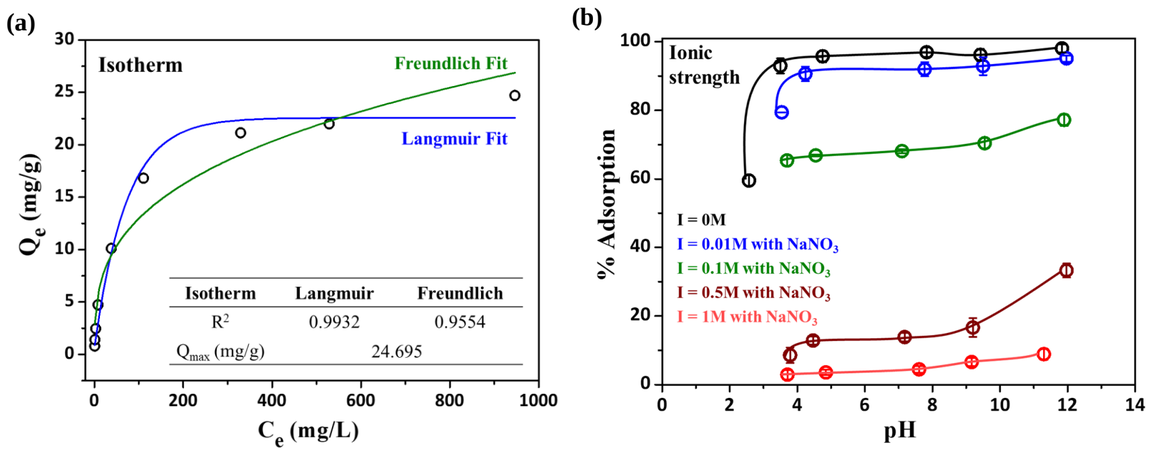

Figure 9. (a) Langmuir and Freundlich models of Ba adsorption on Na-Bentonil; (b) Ionic strength for Ba on Na-Bentonil at different pH.

Experimental Interpretation

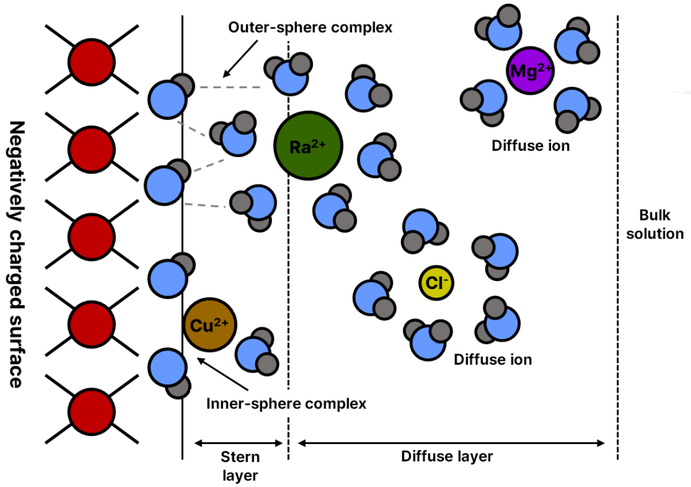

Outer-sphere complexes, stabilized via electrostatic forces across the **Stern layer**, exhibit pronounced sensitivity to ionic strength perturbations.

* At high pH (pH > 9),
- Increased OH^- concentration leads to more OH–water complexes.
- Hydrated OH^- may modify surface charge distribution.

"To further confirm the adsorption mechanism, **DFT** calculations were performed."

*Ref: Liu, Y., et al., Mechanical effect of clay under the acid-base action: A case study on montmorillonite and illite, *Frontiers in Earth Science*, 10, 2022.

Computational methodology

Computational details

1. Exchange-correlation functional: PBE with DFT-D3 method.
2. For geometry, cutoff of 400 eV, EDIFF of 10^{-6} eV.
3. For SCF, cutoff of 600 eV, EDIFF of 10^{-6} eV.
4. For bulk, Monkhorst–Pack method with a 6 × 4 × 3 kpoints.
5. For hydrate system, 15 × 15 × 15 Å^3 unit cell with Γ-point sampling.

❖ Bulk structure and Slab model

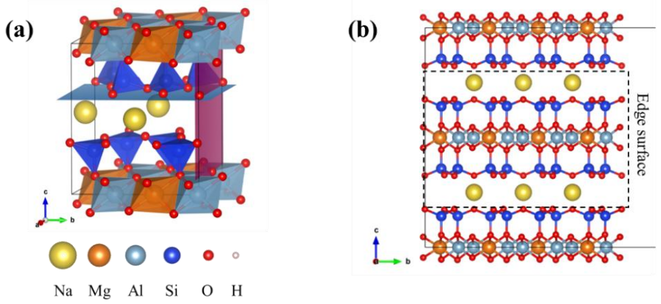

- Optimized lattice parameters of MMT
  a = 5.03 Å, b = 8.68 Å, c = 9.81 Å,
  α, γ = 90.00° and β = 98.55°

⬍

- Lattice parameters of MMT from Exp.
  a = 5.18 Å, b = 8.98 Å, c = 10.10 Å
  α, γ = 90.00° and β = 99.6°

Figure 10. Schematic of the MMT structure: (a) optimized unit cell; (b) unit cell expansion for the (010) slab model.

Radium in aqueous system

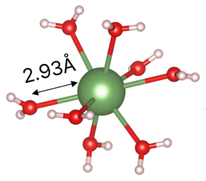

$[Ra(H_2O)_8]^{2+}$

$[Ra(H_2O)_8]^{2+}$
as the most stable species

Coordination beyond 8 water molecules involves movement of the excess ligand beyond the first hydration shell.

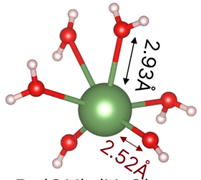

$Ra(OH)_2(H_2O)_4$

$Ra(OH)_2(H_2O)_4$
as the most stable species

Due to steric effects, water molecules beyond the coordination number of 6 are separated from the first hydration shell.

💡 Select only the water molecules that entered the first hydration cell

Surface depending on pH

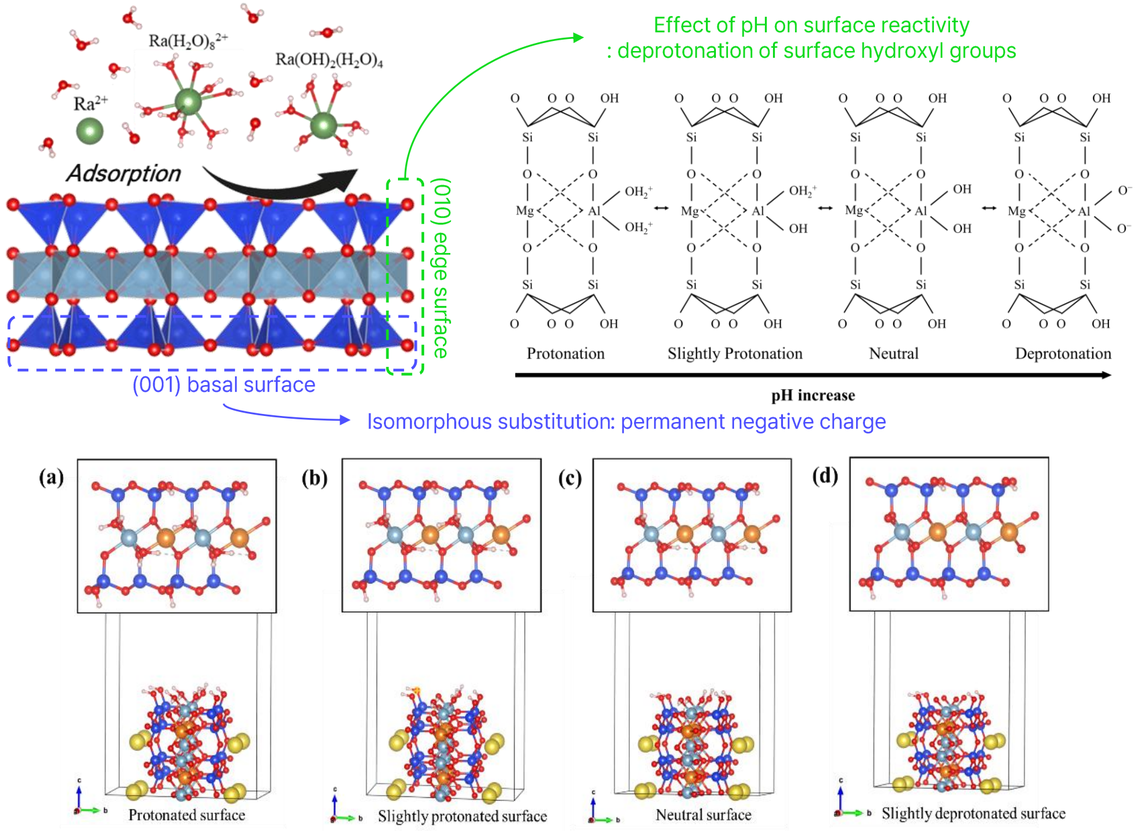

Figure 11. Optimized slab models of the MMT (010) edge surface at different pH.

Adsorption energy

$$\Delta E_{ads} = E_{total} - (E_{slab} + E_{Ra(Ba)-complex})$$

where E_{total} represents the total energy of the system following adsorption, while E_{slab} and $E_{Ra(Ba)-complex}$ correspond to the energies of the MMT slab model and the hydrated or hydroxyl-hydrated Ra- or Ba-complex, respectively.

∴ A negative ΔE_{ads} indicates that the adsorption process is thermodynamically favorable

Results and discussions

Radium Adsorbed on MMT (001) surface

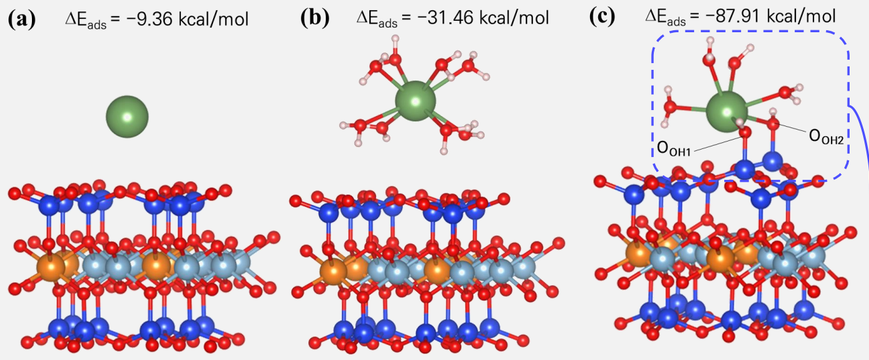

Figure 12. Adsorption configurations and energies of (a) Ra^{2+}, (b) $Ra(H_2O)_8^{2+}$, and (c) $Ra(OH)_2(H_2O)_4$ on the (001) surface.

⁎ Charge density difference (CDD)

significant increase in electron density over a broad spatial range perpendicular to the surface Si–O.

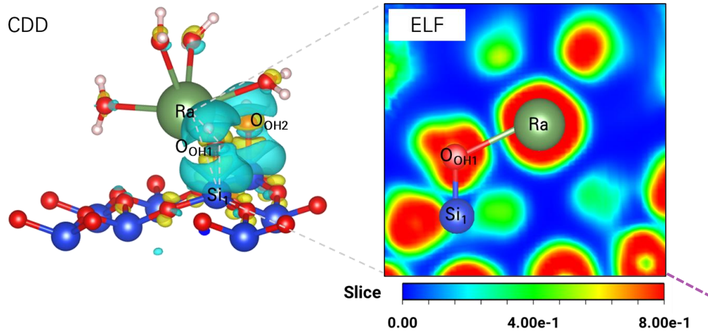

Function of the Ra height

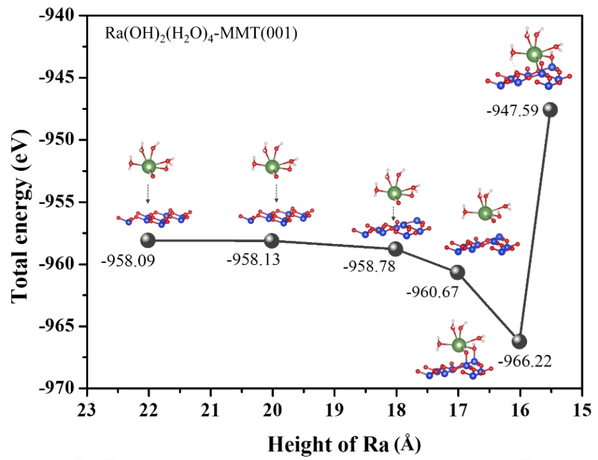

Figure 13. Total energy change as a function of the Ra height at ≡SiO site on (001) surface.

Radium Adsorbed on MMT (010) surface

⁎ Charge density difference (CDD)

perpendicular redistribution of electrons between Ra–O_{SR} occurred at the ≡AlOH sites

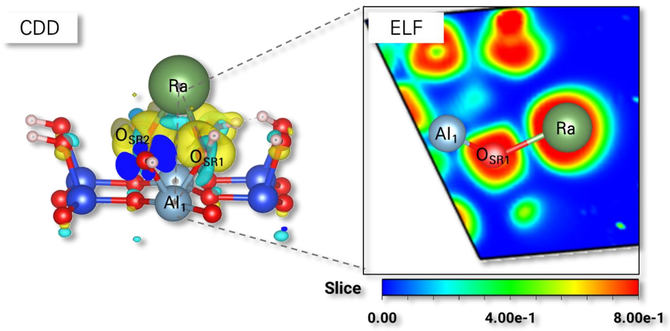

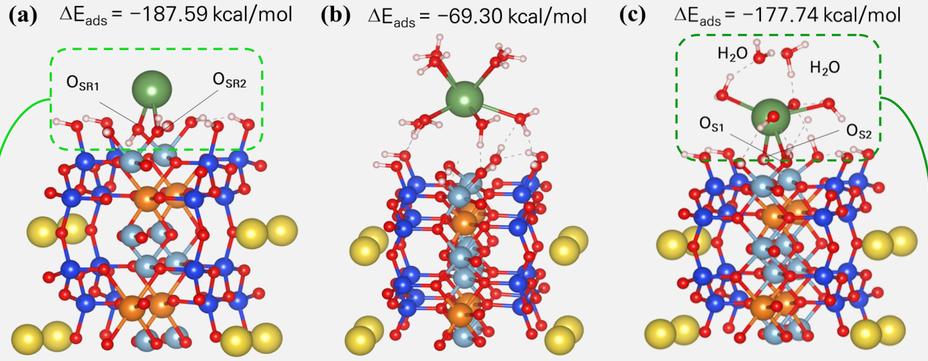

Figure 14. Adsorption configurations and energies of (a) Ra^{2+}, (b) $Ra(H_2O)_8^{2+}$, and (c) $Ra(OH)_2(H_2O)_4$ on the (010) surface.

⁎ Charge density difference (CDD)

Small electron transfer indicating hydrogen bonding
+
significant electron redistribution

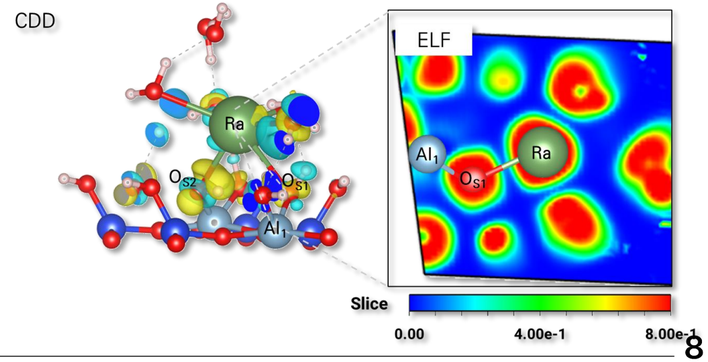

Results and discussions

Radium Adsorbed on MMT (010) surface depending on pH

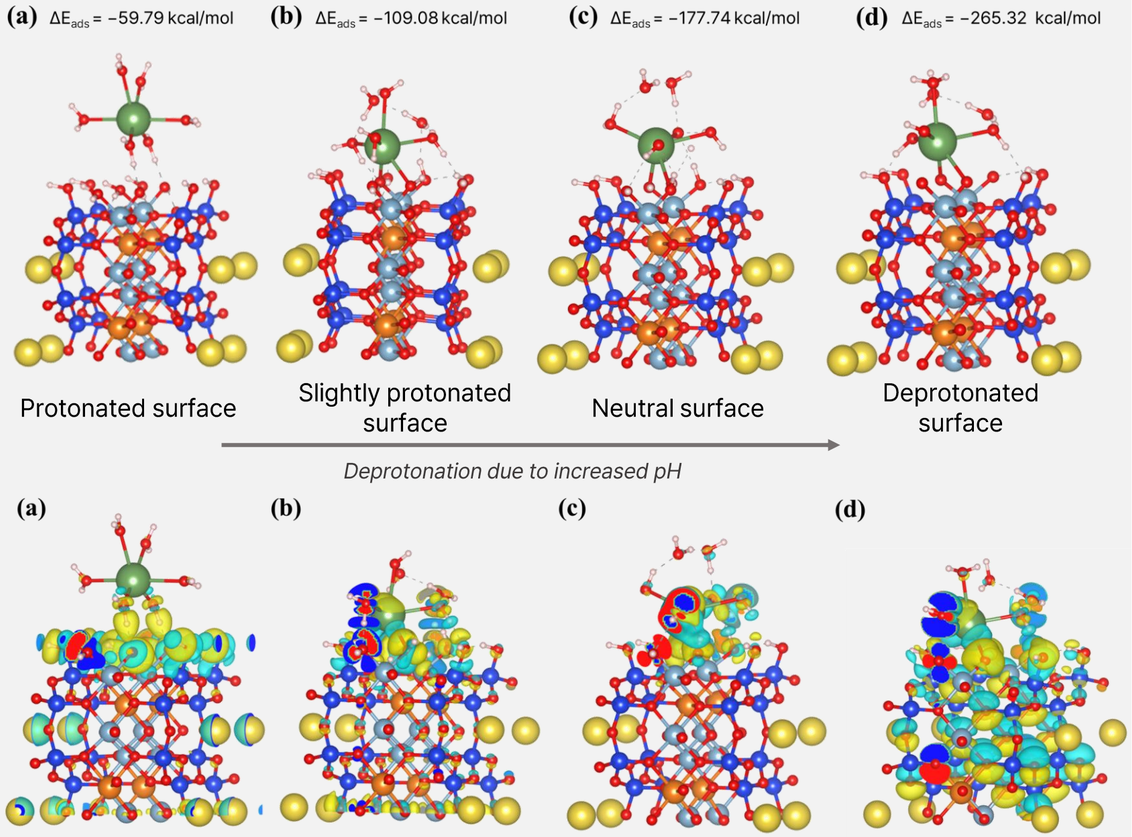

Figure 15. Adsorption configurations and charge distribution of $Ra(OH)_2(H_2O)_4$ on (a) protonated, (b) slightly protonated, (c) neutral, and (d) deprotonated surface as a function of pH.

$\equiv SOH \leftrightarrow \equiv SO^- + H^+$

$\equiv SOH + H^+ \leftrightarrow \equiv SOH_2^+$

At higher pH, deprotonated hydroxyl groups ($-O^-$) enhance the binding affinity for Ra and Ba.

Type of adsorbed Ra on MMT surface ⇔ **Type of adsorbed Ba on MMT surface**

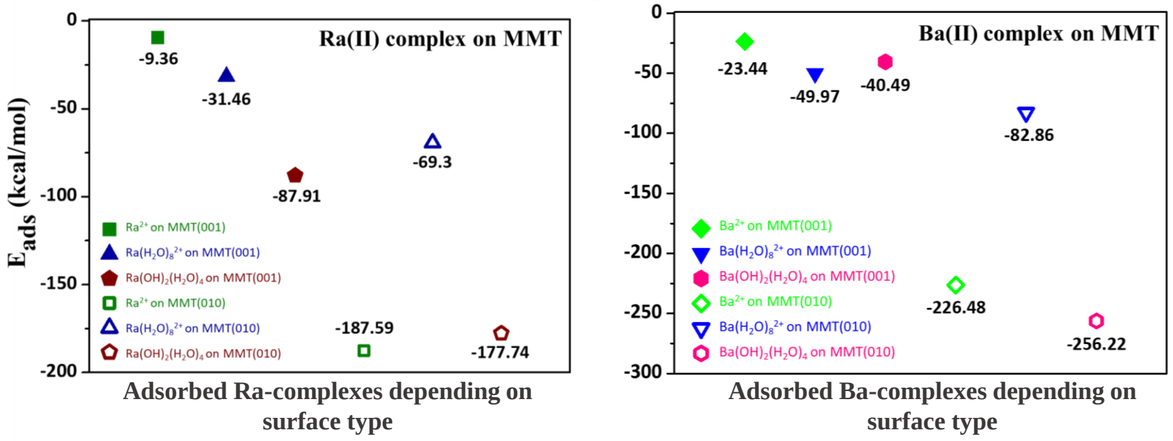

Figure 16. (a) Comparison of Ba and Ra adsorption energies on different MMT surfaces.

⁎ Experimental study from EXAFS*

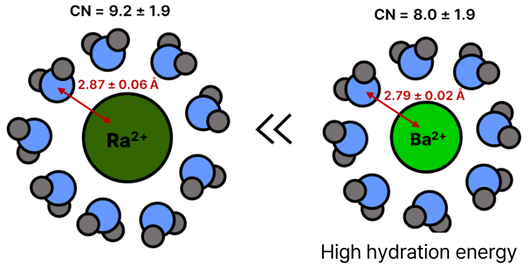

For the (001) surface,
1. $Ba^{2+} > Ra^{2+}$
2. $Ba(H_2O)_8^{2+} > Ra(H_2O)_8^{2+}$

} Steric effect

3. $Ba(OH)_2(H_2O)_4 < Ra(OH)_2(H_2O)_4$ → Weak hydration energy

For the (010) surface,
1. $Ba^{2+} > Ra^{2+}$
2. $Ba(H_2O)_8^{2+} > Ra(H_2O)_8^{2+}$ → Steric effect
3. $Ba(OH)_2(H_2O)_4 > Ra(OH)_2(H_2O)_4$

⁎ Significance of edge surfaces

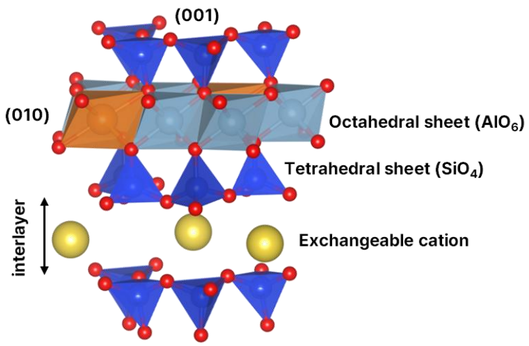

Although (010) surfaces account for only ~10% of the total surface area, they are highly reactive due to exposed hydroxyl groups, enabling strong binding with cations.

*Ref: Yamaguchi, A., et al., Extended X-ray absorption fine structure spectroscopy measurements and ab initio molecular dynamics simulations reveal the hydration structure of the radium(II) ion. *iScience*, 25(8), 104763, 2022.

Results and discussions

Projected Density of States (PDOS)

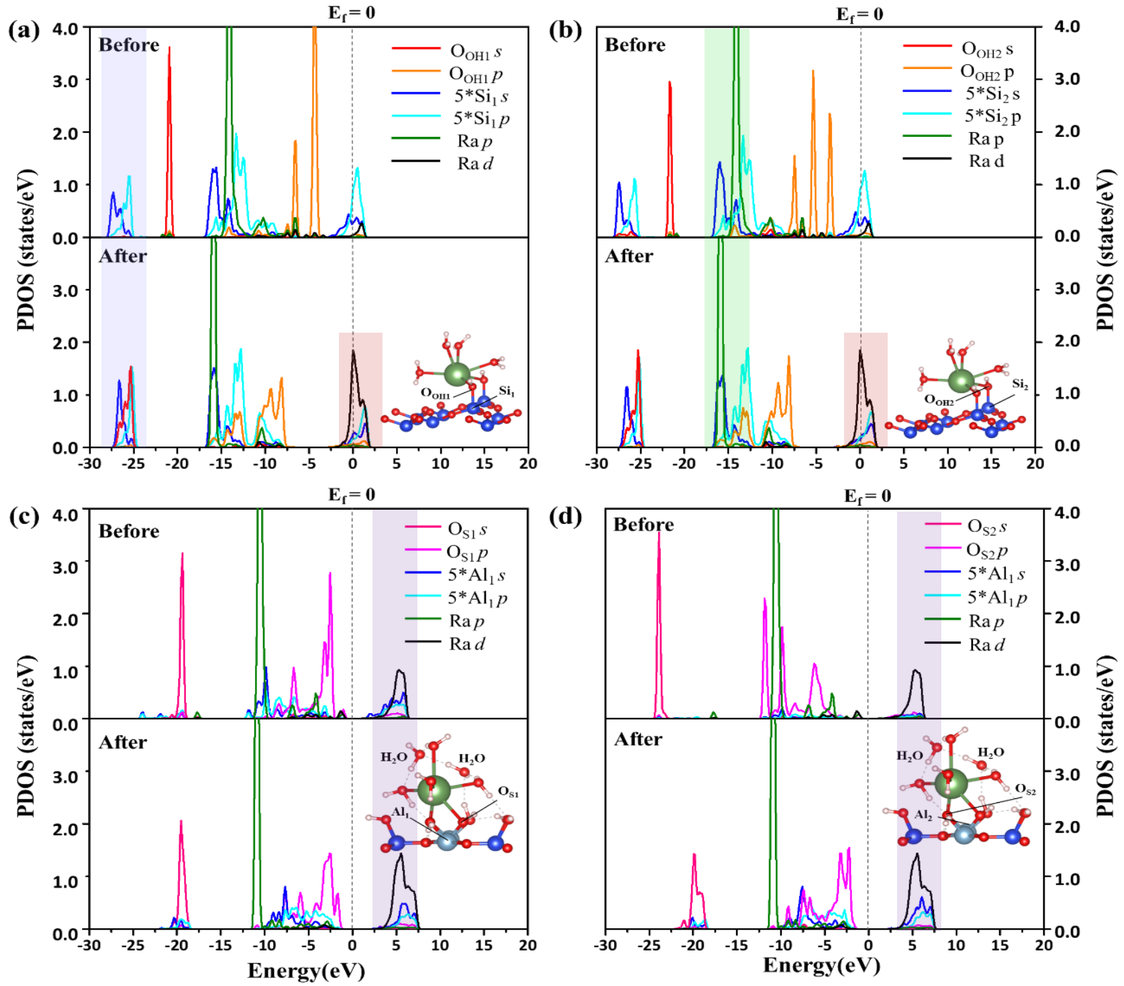

Figure 17. The projected density of state (PDOS) before and after adsorption. Plotted as PDOS of Si multiplied by 5. (a and b) $Ra(OH)_2(H_2O)_4$ adsorbed on (001) basal surface. (c and d) $Ra(OH)_2(H_2O)_4$ adsorbed on (010) edge surface. The Fermi energy was set to zero for all PDOS plots.

PDOS Interpretation

⁎ For the (001) surface with $Ra(OH)_2(H_2O)_4$

- **Before adsorption**: Minimal overlap between Si 3s/3p and O_{OH1} 2s orbitals.
- **After adsorption**:
  - Complete overlap between Si 3s/3p and O_{OH1} in the −29 to −24.5 eV range, indicating strong chemical bonding.
  - Ra 6p orbitals shift to lower energies and overlap with O_{OH1} → suggests enhanced stability.
  - Ra 5d orbitals split into two peaks near the Fermi level, suggesting significant involvement in bonding, possibly due to relativistic effects.

⁎ For the (010) surface with $Ra(OH)_2(H_2O)_4$

- **Before adsorption**: Ra orbitals do not participate in bonding; only Al–O overlaps are observed.
- **After adsorption**:
  - Slight overlap of Ra 6p with Al and O_{SR} orbitals in the 1.1–6.0 eV range → indicates hybridization.
  - Ra 5d orbitals show splitting near 3.25 eV, confirming their contribution to bonding.
  - A weak overlap of Ra 6p with Al and O orbitals is observed in the −5 to 3.2 eV range, implying formation of bonding interactions not present before adsorption.

Theoretical and Experimental Investigation of Radium Adsorption Mechanisms on Engineered Barrier Material

Summary of this study

This study integrated DFT calculations and batch adsorption experiments to understand how Ra interacts with MMT surfaces.

Key findings include:

- **$Ra(OH)_2(H_2O)_4$** showed the most stable adsorption form on both surfaces, particularly strong on the (010) surface due to interactions with surface hydroxyl groups.
- **Ra^{2+}** and **$[Ra(H_2O)_8]^{2+}$** mostly form weaker outer-sphere complexes through electrostatic or hydrogen bonding.
- **Batch adsorption experiments** showed pH-dependent adsorption, with higher Ra uptake at high pH, supporting the theoretical prediction that Ra adsorption is stronger on deprotonated (high pH) surfaces.
- **PDOS and charge density analyses** confirmed that Ra binding is stabilized through orbital overlap and charge transfer, especially on hydroxyl-rich surfaces.

Overall, these findings demonstrate that the edge surface plays a crucial role in Ra retention. Under high-pH conditions induced by cement and surrounding rock, Ra is expected to exhibit enhanced adsorption affinity, thereby improving its retention in deep geological repositories.

KNS Spring Meeting 2025

Thank you for your kind attention

경청해 주셔서 감사합니다.

Jaeeun Kang*

*jenny94@postech.ac.kr

Nuclear Environmental Laboratory (NEL)
Division of Advanced Nuclear Engineering (DANE), POSTECH